

## Biopsy needle detection in transrectal ultrasound

Alper Ayvaci<sup>a</sup>, Pingkun Yan<sup>b,\*</sup>, Sheng Xu<sup>c</sup>, Stefano Soatto<sup>a</sup>, Jochen Kruecker<sup>c</sup>

<sup>a</sup> University of California, 405 Hilgard Ave, Los Angeles, CA 90095, USA

<sup>b</sup> Center for OPTical IMagery Analysis and Learning (OPTIMAL), State Key Laboratory of Transient Optics and Photonics, Xi'an Institute of Optics and Precision Mechanics, Chinese Academy of Sciences, China

<sup>c</sup> Philips Research North America, 345 Scarborough Rd, Briarcliff Manor, NY 10510, USA

### ARTICLE INFO

#### Article history:

Received 23 July 2010

Received in revised form 18 March 2011

Accepted 24 March 2011

#### Keywords:

Needle detection

Interventional guidance

Prostate

Transrectal ultrasound

Fusion

Prior knowledge

### ABSTRACT

Using the fusion of pre-operative MRI and real time intra-procedural transrectal ultrasound (TRUS) to guide prostate biopsy has been shown as a very promising approach to yield better clinical outcome than the routinely performed TRUS only guided biopsy. In several situations of the MRI/TRUS fusion guided biopsy, it is important to know the exact location of the deployed biopsy needle, which is imaged in the TRUS video. In this paper, we present a method to automatically detect and segment the biopsy needle in TRUS. To achieve this goal, we propose to combine information from multiple resources, including ultrasound probe stability, TRUS video background model, and the prior knowledge of needle orientation and position. The proposed algorithm was tested on TRUS video sequences which have in total more than 25,000 frames. The needle deployments were successfully detected and segmented in the sequences with high accuracy and low false-positive detection rate.

© 2011 Elsevier Ltd. All rights reserved.

### 1. Introduction

Prostate cancer affects one in six men in the western world, and it is the second leading cause of cancer death in American men [1]. Currently, patients are being diagnosed using a so-called “blind” transrectal ultrasound (TRUS)-guided systematic biopsy [2]. Ultrasound imaging, however, merely guides the needle to different regions of the prostate, and does not visualize prostate cancer reliably. On the other side, multi-parametric MRI has been shown to have good sensitivity and specificity in detecting prostate cancer. Efforts have been made to create image guidance applications that can fuse real-time TRUS with pre-acquired MRI to guide needles to diagnostic or therapeutic target sites identified in MRI [3,4].

In MRI/TRUS fusion guided targeted prostate biopsy and therapy, there are several situations in which it is important to know the exact location of the deployment of the biopsy needle. First, biopsy needle tip localization plays an important role in retrospective analysis of the image fusion system. In prostate biopsy, the biopsy needle is deployed by using a biopsy gun. The needle tip for tissue sampling may not exactly hit the planned target site. It would be very useful to find the actual biopsy locations in a procedure and then map to the MR images. The targets identified on multi-parametric MR can then be correctly correlated with the

pathological analysis results. Second, for repeat biopsies, physicians may either want to re-sample regions with suspicious findings in earlier biopsies, or may want to specifically avoid re-sampling regions with benign findings and target areas in between previous biopsies instead. In both cases, the exact locations of earlier biopsy samples need to be known. Furthermore, locations of the positive biopsies are needed in addition to imaging findings for planning focal therapy.

This paper presents a new method for robustly detecting and accurately segmenting the biopsy needle from 2D TRUS videos recorded during the MRI/TRUS fusion guided biopsy procedures. Since the biopsy needle is setup to be in the imaging plane of the ultrasound probe, it appears as a tubular structure at the deployment time. Needle detection and segmentation in TRUS, however, is a very challenging task for the following reasons. First of all, it is well known that ultrasound has low signal to noise ratio and the noise makes the boundary of the needle difficult to define. Second, the biopsy needle, which appears to be a bright tubular structure in ultrasound, is often surrounded by other bright anatomical structures with a similar intensity profile (as shown in Fig. 1). Third, the possibility of out-of-plane bending of the needle further reduces the needle visibility in TRUS images. Last but not least, since the needle is fired by a biopsy gun, it appears in the TRUS images suddenly and lasts only several frames. The sudden needle motion plus the motion caused by the movement of the US probe makes needle detection even more difficult.

The problem of biopsy needle segmentation from ultrasound has been investigated recently. Naturally, the majority of the proposed segmentation algorithms exploit the linear and tubular structure of

\* Corresponding author.

E-mail addresses: [ayvaci@cs.ucla.edu](mailto:ayvaci@cs.ucla.edu) (A. Ayvaci), [pingkun.yan@opt.ac.cn](mailto:pingkun.yan@opt.ac.cn) (P. Yan), [sheng.xu@philips.com](mailto:sheng.xu@philips.com) (S. Xu), [soatto@cs.ucla.edu](mailto:soatto@cs.ucla.edu) (S. Soatto), [jochen.kruecker@philips.com](mailto:jochen.kruecker@philips.com) (J. Kruecker).



Fig. 1. TRUS image with needle deployment.

the needle to segment it. Wei et al. [5,6] first threshold the image, and subsequently, fit a line to the points determined by thresholding. Draper et al. [7] follows similar steps and starts from a thresholded image and apply morphological operations to fill the gaps, and fits a tubular model using Principal Component Analysis (PCA). Another choice for detection of needle is the Hough transform, as it is one of the earliest methods to find linear structures. The performance of these methods highly depends on preprocessing steps which can have poor results especially in the case of ultrasound images. For example, Hough transform was used in the work of [8–10] after applying morphological operations on the image. However, similar to line fitting, the nature of the Hough transform makes these methods prone to the problems mentioned earlier, especially the out-of-plane bending of the needle and the distraction from the surrounding bright structures. In addition, all the existing methods assume presence of biopsy needle in the images.

In this paper, we present a new method to detect the biopsy needle in TRUS video sequences recorded during actual MRI/TRUS fusion-guided biopsies. To achieve better robustness and accuracy, we propose to combine information from multiple resources, including ultrasound probe stability, TRUS video background model, and the prior knowledge of needle orientation and position for detection. In the proposed method, we first detect the needle deployment in ultrasound videos. Then for those TRUS frames where the needle is present, we segment the needle to further verify its presence. To the best of our knowledge, this is the first method to detect the biopsy needle deployment from TRUS videos recorded during the biopsy procedures.

The rest of the paper is organized as follows. Section 2 provides an overview of the MRI/TRUS fusion guided biopsy system. The proposed biopsy needle detection method using multi-source information fusion is presented in Section 3. The prior knowledge based needle segmentation algorithm is presented in Section 4. In Section 5, the performance of the proposed detection and segmentation methods is demonstrated on biopsy TRUS video sequences with quantitative evaluation results. Finally, Section 6 concludes the paper.

## 2. MRI/TRUS fusion guidance

A system for fusion of real-time transrectal ultrasound (TRUS) with pre-acquired 3D images of the prostate was designed and demonstrated in our previous work [3]. Biopsy guides for endocavity ultrasound transducers were equipped with customized 6 degree-of-freedom (DoF) electromagnetic (EM) tracking sensors, compatible with the Aurora EM tracking system (Northern Digital Inc., Waterloo, ON, Canada). The biopsy guides were attached to an ultrasound probe and calibrated to map ultrasound image coordinates to EM tracking coordinates.

EM tracking systems are considered an enabling technology for many image guided procedures since they are not limited by sight restrictions. With the assistance of EM tracking, a transformation chain can be constructed for fusing the real-time TRUS and the pre-acquired MRI as shown in Fig. 2. With those transformations, we are able to find the 3D world locations of the pixels in a 2D TRUS frame.

## 3. Biopsy needle detection

Automatic biopsy needle deployment detection from TRUS video is a very challenging problem. To deal with the aforementioned difficulties, we propose to detect biopsy needle deployment by integrating the multi-source information of ultrasound probe stability, TRUS video background model, and the prior knowledge of needle orientation and position. The proposed method consists of three main steps. First, we use the EM-tracking information from the ultrasound probe sensor to segment the video into sections in which the ultrasound probe appears stationary. Second, we highlight the needle using a filter specifically designed to respond to the biopsy needle inside an image. Third, we detect the scene changes with respect to a background model that is maintained throughout each video segment. By combining all the three steps together, the presence of the biopsy needle can be detected. The details of each step are presented as follows.

### 3.1. Quantifying probe stability

It has been observed that during the biopsy, urologists stabilize the ultrasound probe before they deploy the needle to get a tissue sample from the prostate. This observation helps us to narrow down the search space of the needle deployment time, which can significantly speed up the detection process and also reduce the false positive rate. In other words, we consider only the frames where the ultrasound probe is relatively stationary for the needle detection and segmentation.

Although it is possible to use the TRUS frames directly to determine whether the probe is stationary, using images only is not reliable in our application. The most important reason is that the TRUS images are in 2D. Any small out-of-plane motion will cause the image content to be quite different and thus confuse the motion quantification algorithm. To robustly quantify the stability of the ultrasound probe, the EM tracking information, which is collected as a part of the interventional guidance system logging, is used in our work instead. In our approach, we first pick  $N$  points on the TRUS image plane. Then, we find the world coordinates of these points through the position and pose of the probe tracked by the EM tracking system. For each point, we compute the angular distance between the 3D world position of that point and its 3D world position at the previous frame. By comparing the 3D coordinates of the same set of pixels in consecutive frames, we can determine the motion of the US probe. If none of these  $N$  points moves significantly, we tag the frame as “stationary” and thus make the frame a candidate for needle detection.

### 3.2. Enhancing needle structure

Once the TRUS frames which may be captured when the ultrasound probe being stable are identified, needle detection is performed in those frames. However, due to the low signal to noise ratio of TRUS video and other bright structures around the needle with similar intensity profile, using the intensity values of the frame directly cannot produce accurate results. To overcome these problems, we propose to enhance the needle appearance in the images by convolving the TRUS images with a filter, which is specifically designed for exploiting the tubular structure of the needle and

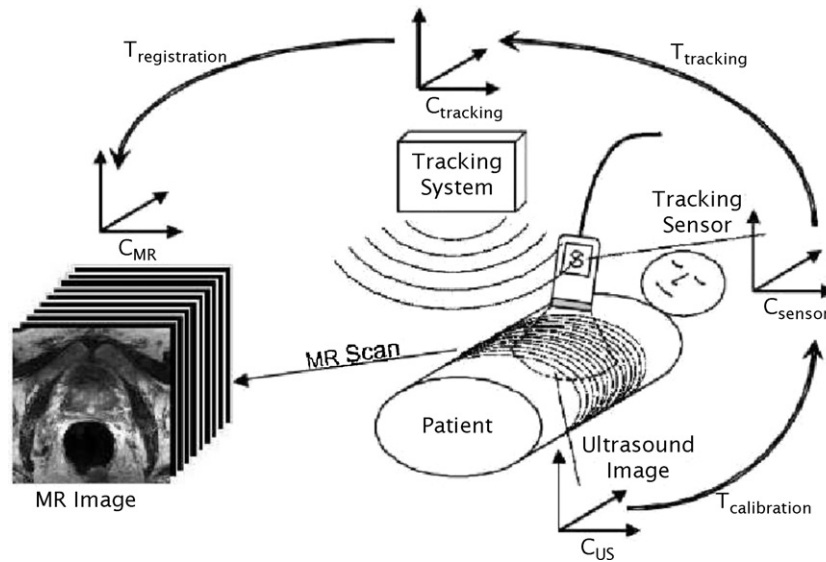


**Fig. 2.** The MR image and the real-time TRUS are mapped together in the EM tracking coordinates for fusion. With the illustrated transformation chain of the MRI/TRUS fusion guided biopsy system, pixels in a TRUS frame can be corresponded to the voxels in the MRI volume.

suppressing the imaging noise in the same time. The second order derivative of Gaussian filter is very suitable for our design. In 2D, the filter can be formulated as

$$G''(x, y) = 2 \left( \frac{2x^2 - 1}{\sigma_x} + \frac{2y^2 - 1}{\sigma_y} \right) \exp \left( -\frac{x^2}{\sigma_x} - \frac{y^2}{\sigma_y} \right), \quad (1)$$

where  $\sigma_x, \sigma_y$  are the variation in  $x, y$  directions, respectively. To exploit the tubular structure of the needle, the values of  $\sigma_x$  and  $\sigma_y$  are selected in a way that  $\sigma_y \gg \sigma_x$ . Fig. 3 shows the shape of the designed enhancement filter in 3D. The response of the filter is low on the needle and is high at other places. To increase the filter response, we also rotate the filter to align its orientation to the needle guide by multiplying by a 2D rotation matrix. Some response images of the filter to needles deployed at different times are shown in Fig. 4. Note that even though the needle signal is weak in the second and third examples, a noticeable filter response is still obtained on the needle.

### 3.3. Modeling image background

After filtering the candidate TRUS images using the needle enhancement filter, we move to detect the needle deployment in the enhanced frames. Since the needle is fired by a biopsy gun, it appears in the TRUS images suddenly and lasts only several frames. When the ultrasound probe is stable, the only significant change happening in the scene is caused by the needle deployment as the respiratory motion can be ignored compared with the sudden needle motion. To detect the fired needle in TRUS, we propose to model the image background and check the difference between the current image and the model. Large difference may indicate the sudden appearance of the needle.

In our proposed approach, the histogram of the filter response is used for background modeling, which can represent the filter response intensity information and is also invariant to the small respiratory motion. Let  $H(t)$  be the standard spatial histogram of the filter response, aggregated over all the pixels in a fixed region around the biopsy guide at frame  $t$ . In our work, the minimum and maximum values of the filter response are  $-255$  and  $+255$ , respectively. The range is uniformly divided into 100 equally spaced bins to construct the histograms. For the first frame of the stable video segment, we model the background directly with its histogram as  $B(t_0) = H(t_0)$ . To maintain the background model in the following

frames, the histogram is incrementally updated using a new frame as

$$B(t) = \alpha B(t-1) + (1-\alpha)H(t), \quad (2)$$

where  $\alpha$  is the learning rate. Typically, we choose  $\alpha$  as 0.9 to maintain the continuity of the model but also to quickly learn the new images.

To detect changes in the scene using the background model, the distance between the background model  $B(t-1)$  and the histogram of filter responses  $H(t)$  is measured by using  $\ell_1$  norm of their difference. When the distance is larger than a threshold, the frame  $t$  is considered as significantly varying from the background model and marked as the *candidate needle frames*.

### 4. Biopsy needle segmentation

The change detection algorithm described in the previous section not only marks the frames with needle deployment but also rejects many false-positive frames, where there is no needle appearance. After that, the biopsy needle segmentation is carried out for locating the needle tip and also further eliminating the remaining false positives by verifying the presence of needle in an image.

For efficient and accurate segmentation, a two step segmentation algorithm based on minimizing an energy function using the graph-cuts method is proposed [11–13]. First, the image is segmented into needle pieces and background using the filter response. However, this step returns more than one segment for several reasons. One of the causes is that the out-of-plane bending of the needle may reduce the needle visibility in some parts. Another reason is that the bright anatomical structures surrounding the needle may also generate weak filter response, which can be captured by the initial segmentation algorithm. To deal with this problem, in the second step, these segments are clustered based on the prior knowledge of the position and orientation of the needle guide. In addition, the clustering of the pieces that form a tubular structure is favored. A modified graph-cuts method is used for this purpose.

Once we have the segmentation of the needle, we can further eliminate false positives based on the obtained shape, orientation and its position with respect to the needle guide. This approach helps us to reliably eliminate a large number of the candidate nee-

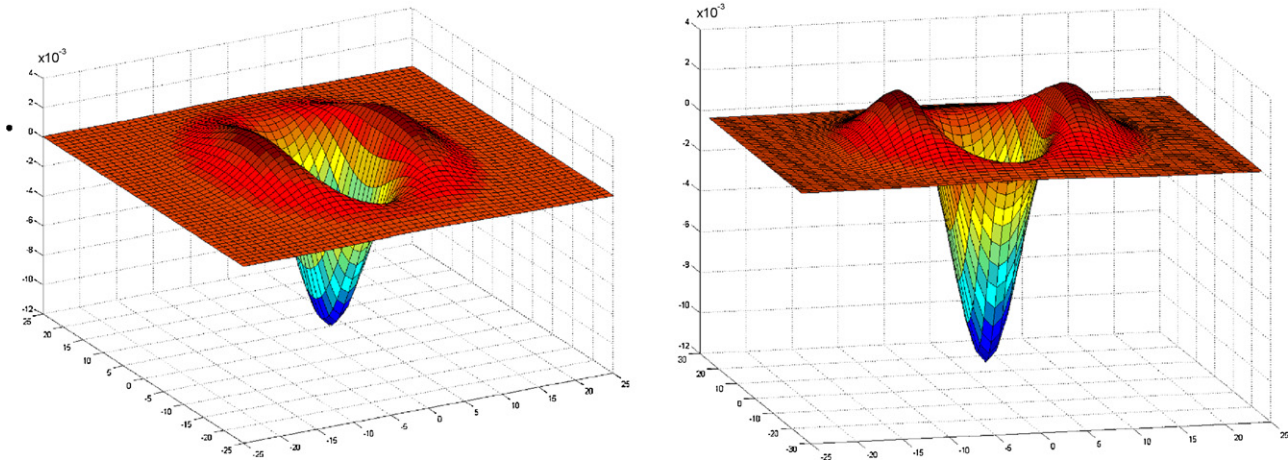


Fig. 3. The 3D shape of the second order derivative Gaussian filter in different views.

dle frames actually without needle deployment. The details of the proposed method are provided in the following subsections.

#### 4.1. Segmenting images

Consider a needle as foreground and other structures as background. The problem of segmenting a frame with possibly a needle inside can be formulated as the minimization of an energy functional

$$\hat{x}_p = \underset{(x_p)}{\operatorname{argmin}} \sum_p D_p(x_p) + \lambda \sum_{p \sim q} w_{pq} [x_p \neq x_q], \quad (3)$$

where  $x_p$  is the binary label of the pixel  $p$ , and  $p \sim q$  indicates that the pixels  $p$  and  $q$  are neighbors. The first term of the energy functional  $D_p(x_p)$  describes the cost of assigning a pixel  $p$  to the foreground or to the background based on its label. The cost of assigning a pixel to the foreground is chosen as the absolute difference between the filter response  $f_p$  at that pixel and the minimum filter response  $\epsilon$  of the image. This cost achieves its minimum value at the pixels inside the needle as the filter that enhances the needle gives its lowest response at those pixels. In a similar way, the cost of assigning a pixel to the background is chosen as the absolute difference between the filter response  $f_p$  at that pixel and the mean filter response  $\mu$  of the image.

The second term on the right-hand side of the energy functional regularizes the labeling to maintain the smoothness of the segmentation with the multiplier factor  $\lambda$ . When two neighboring

pixels,  $p$  and  $q$ , have different labels  $x_p$  and  $x_q$ , the prediction of  $[x_p \neq x_q]$  takes the value of 1 and the weight  $w_{pq}$  accumulates to the energy. Otherwise, it takes the value of 0 and the weight  $w_{pq}$  has no contribution to the total energy. As a natural choice for  $w_{pq}$  that favors the assignment of the same label to the neighboring pixels with similar filter responses, the similarity measure is chosen to be  $w_{pq} = \exp(-\beta|f_p - f_q|)$ .

By using the above formulation, an image gets segmented when the energy functional in (3) is minimized. To find the global minimum, the graph-cuts based minimization is employed as the form of the energy functional is well suited to be formulated as a graph-cut problem. Fig. 5 shows the graph constructed corresponding to the energy functional in (3). The graph can be constructed in three steps. First, a node is put into the graph for each pixel. Second, as this is a binary optimization problem, two terminal nodes  $s$  and  $t$  representing background and foreground are added. Third, the terminal node  $s$  is connected to each node representing the pixels using edges with the weight of  $|f_p - \epsilon|$ , and the terminal node  $t$  is connected to each node with the weight of  $|f_p - \mu|$  to those edges in a similar way. Finally, edges that connect the nodes representing neighboring pixels are added and assigned the weight of  $w_{pq}$ .

The minimum cut on this graph generates the labeling that globally minimizes the energy functional in (3). It is worth noting that the minimal cut can be computed in polynomial time. Therefore it is computationally an efficient method for energy minimize. Fig. 6 illustrates the segmentation of the needles from the ultrasound frames with our approach.

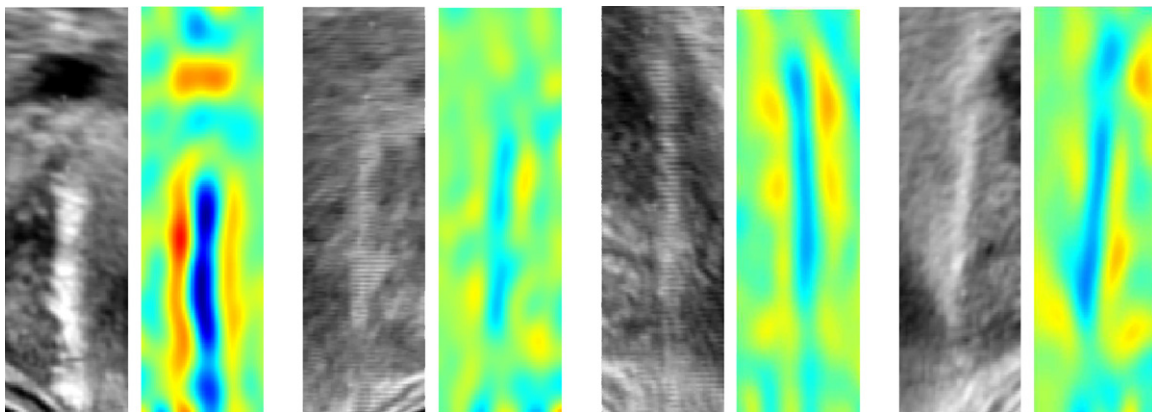


Fig. 4. Four filter response examples of the needle structure enhancement. For each example, the TRUS image patch is shown on the left and the color-coded enhancement result is shown on the right. The color scale is from blue to red indicating the values from low to high. The lower response values point out the existence of a tubular structure. (For interpretation of the references to color in this figure legend, the reader is referred to the web version of the article.)

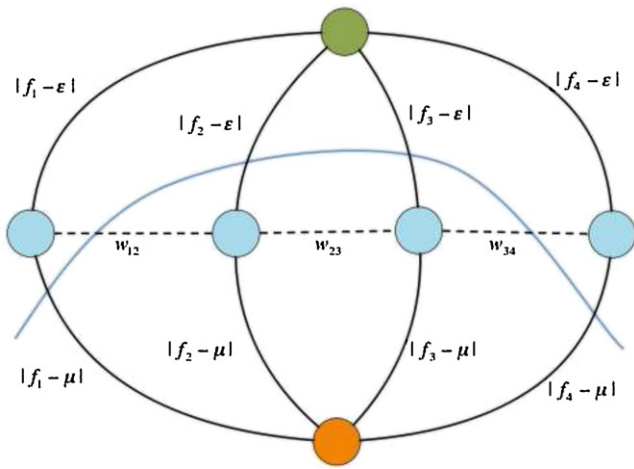


Fig. 5. The constructed graph corresponding to the energy functional in (3).

4.2. Clustering segments

For a clear needle deployment, it is relatively easy to segment from the filter response image. However, sometimes only part

of the needle is visible in the scene, especially when a needle is deployed partially out of the imaging plane due to bending. In that situation, the segmentation algorithm described at the previous section will return multiple needle fragments as shown in Fig. 7(b). To overcome this problem, we propose a clustering algorithm using the prior knowledge of the needle shape and the needle guide, through which the needle is deployed.

To utilize the position and orientation of the needle guide for a more robust segmentation, first, a confidence map based on the distance map of the needle guide is computed. The confidence map indicates the possibility of the presence of the biopsy needle at each location. An example of the confidence map is shown in Fig. 7(c). Each pixel  $p$  on this confidence has the value  $c_p = 1 - d_p/d_{max}$ , where  $d_p$  is the distance from the pixel  $p$  to the needle guide and  $d_{max}$  is the maximum distance on the distance map. The closer a pixel to the needle guide, the higher the confidence value is, and vice versa. To evaluate the possibility of each fragment being part of the needle, the confidence value for each segment  $S$  is computed by

$$C_S = \frac{1}{|S|} \sum_{p \in S} c_p, \tag{4}$$

where  $|S|$  is the number of pixels inside  $S$ .

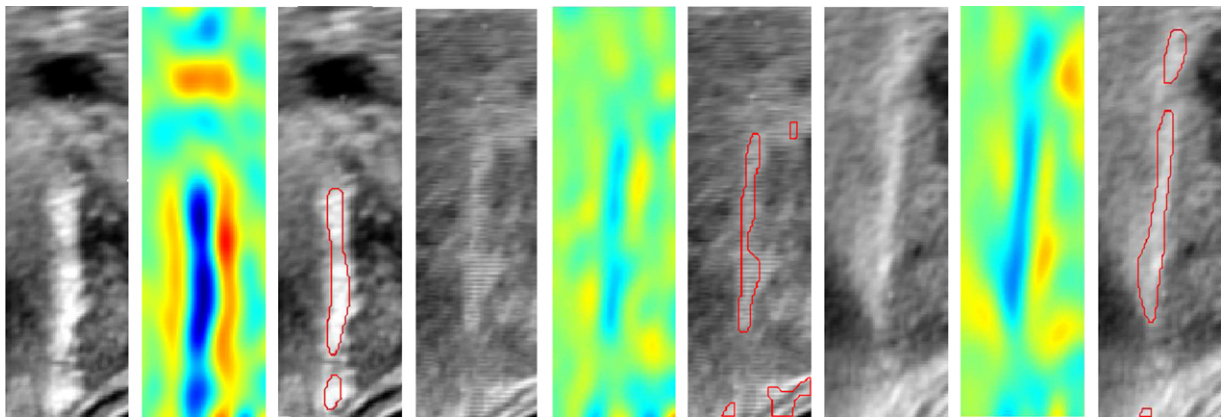


Fig. 6. This figure illustrates the segmentation of needles from the ultrasound frames in three different cases. Each image group shows the input image, filter response and the segmentation of the needle.

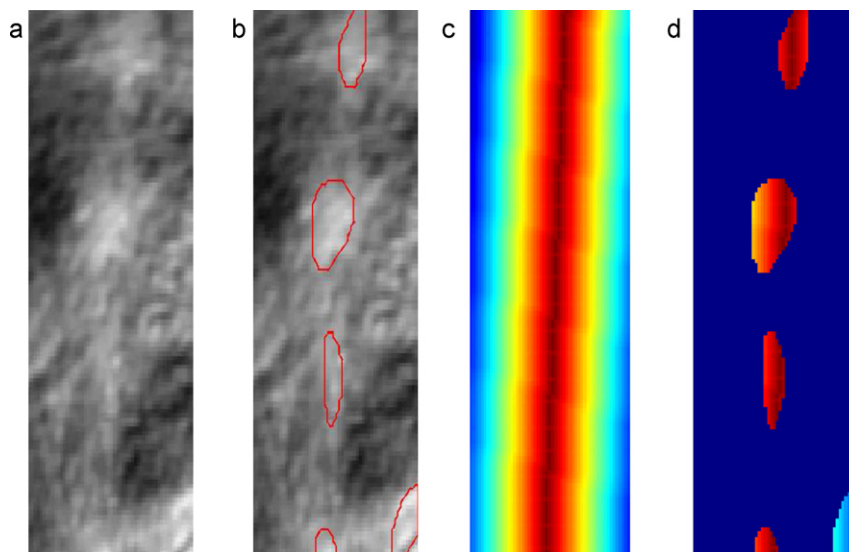


Fig. 7. Illustration of the needle segmentation process: (a) the needle appears partially in the image because of the out-of-plane deployment; (b) fragmented segmentation of the needle obtained by graph-cuts; (c) confidence map computed based on the distance map around the needle guide; and (d) confidence values on each needle fragment.

On the other hand, to exploit the tubular shape of the needle and its orientation, we propose to use the ratio between two principal axes of segments. The orientation of the principal axes and their lengths is given as the eigenvectors and eigenvalues of an inertia matrix

$$M = \begin{bmatrix} m_{20} & m_{11} \\ m_{11} & m_{02} \end{bmatrix}, \tag{5}$$

where

$$m_{pq} = \frac{1}{|S|} \sum_p (x_p - \mu_x)^p (y_p - \mu_y)^q, \tag{6}$$

$x_p$  and  $y_p$  are the coordinates of the pixel  $p$ , and  $\mu_x$  and  $\mu_y$  are the means of  $x$  and  $y$  coordinates, respectively.

Once the confidence value of each segment is computed, the segments can be clustered into needle and non-needle parts based on the minimization of the energy functional

$$\hat{z}_s = \underset{\{z_s\}}{\operatorname{argmin}} \sum_{S \in A} K_S(z_s) + \tau \sum_{S, Q \in A} \frac{R_{SQ}}{D_{SQ}} [z_s \neq z_Q], \tag{7}$$

where  $A$  is the set of segments,  $z_s$  is the label of segment  $S$ ,  $K_S(z_s = 1) = 1 - C_S$  is the cost of assigning the segment  $S$  as a needle piece,  $K_S(z_s = 0) = C_S$  is the cost of assigning the segment as non-needle piece,  $R_{SQ}$  is the principal axes ratio when the segments  $S$  and  $Q$  are merged,  $D_{SQ}$  is the distance between the segments  $S$  and  $Q$ , and  $\tau$  establishes the balance between the unary and pairwise terms. To efficiently solve this clustering problem, the graph-cuts algorithm [11–13] is again used for finding the global minimum of the energy functional in (7). A graph is constructed by considering each fragment as a node as shown in Fig. 8. The needle fragment clustering result is shown in Fig. 7(d).

After clustering the needle fragments, the final step in segmentation is to verify whether the segmented object is a biopsy needle to eliminate the false positives based on the orientation, shape and the position of the segmented object. First, we check the principal axes ratio which is high for tubular structures. The threshold value for this criteria is 5. Second, we exclude the segmentations who are far from the needle guide (with the confidence value  $C_S < 0.85$ ) and whose orientation deviates from the guide significantly (more than  $30^\circ$ ). The parameters are chosen empirically and do not vary throughout our experiments. By thresholding according to these three factors, the vast majority of segmented frames with no needle deployments can be reliably eliminated (Fig. 9).

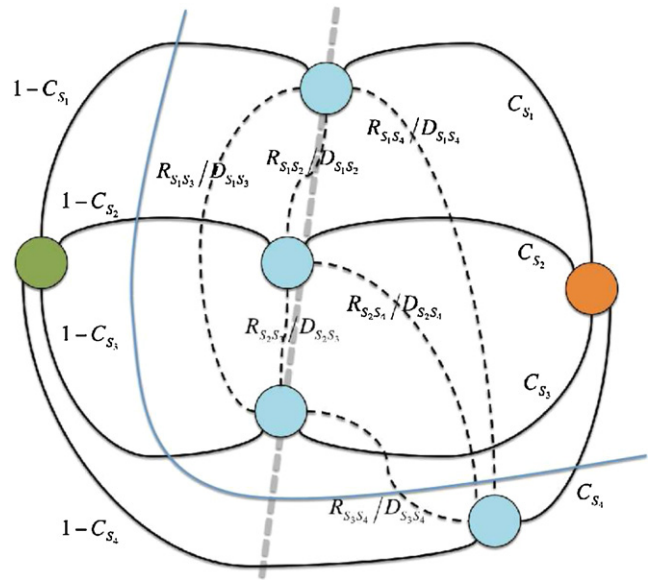


Fig. 8. The graph constructed corresponding to the energy functional (7) for clustering the needle segments.

### 5. Quantitative experiments

Our proposed algorithm has been tested on three TRUS video sequences recorded during the prostate biopsies for patients coming for prostate cancer diagnosis. Ultrasound images used in the experiments were obtained by using an iU22 scanner (Philips Healthcare, Andover, MA). Ultrasound video frames were grabbed by using a video card. Each image has the size of  $640 \times 480$  pixels. The pixel sizes of the frame-grabbed images are 0.1493 mm, 0.1798 mm, and 0.2098 mm for 4 cm, 5 cm, and 6 cm depth settings, respectively. These three video contains more than 25,000 frames, whose details are given in Table 1. The needle deployments identified by a radiologist were considered as the ground truth for evaluation.

Since our main objective is to help the physician to quickly locate the needle deployments for reviewing purpose, a basic requirement is not to miss any needle deployment. For this purpose, we grouped individual needle detections based on temporal coherency and labeled each group as one needle deployment. In the evaluation of our algorithm, we mainly focused on three statistics: the num-

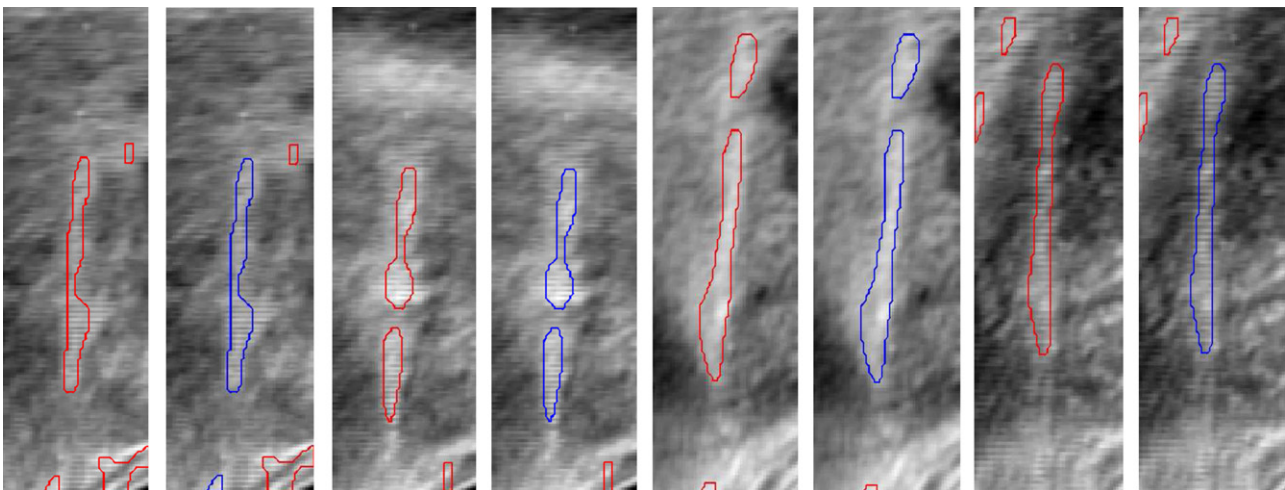


Fig. 9. This figure illustrates the clustering of fragments into one needle segment. The fragments presented with the blue boundary form the needle segment. (For interpretation of the references to color in this figure legend, the reader is referred to the web version of the article.)

**Table 1**

The number of frames, number of needle deployments, number of frames with needle presence, and number of frames without needle presence in the three TRUS video sequences for testing.

Numbers	Sequence-1	Sequence-2	Sequence-3
Frames	2359	12676	10020
Needle deployment	12	16	16
Frames with needle	142	235	243
Frames w/o needle	2217	12441	9777

**Table 2**

This table presents some statistics achieved on Sequence-1, Sequence-2 and Sequence-3 with the proposed algorithm.

	Dataset-1	Dataset-2	Dataset-3
Needle missed	0	0	0
True positives (#)	100	158	130
True positives (%)	70	67	53
False positives (#)	30	327	169
False positives (%)	1.3	2.6	1.7

ber of the missed needles, the percentage of true positives to the number of frames where the needle appears, and the percentage of false positive detections to the number of frames where there is no needle.

Table 2 shows the statistics related to all the three sequences and the performance of the proposed method on them. From the results, we can see that we have achieved the goal of detection of all the needle deployments and no needle deployment was missed.

Even though not all the frames with needle were marked as positive at a needle deployment (the true positive percentage is 70% and 67% for first and second dataset, and 53% for the third one), we were able to detect needle appearance in at least one of the frames during a needle deployment. On the other hand, the false detection rate is very low considering the fact that the needle appears only in a very small percentage of the frames throughout the video. In addition, our investigation showed that the main cause of the false alarms is the needle traces left after needle is fully retracted. Overall, our method has 97% accuracy in classification of the frames into the classes “with needle” and “without needle”.

## 6. Conclusions

This paper presents an algorithm capable of detecting biopsy needle deployments from TRUS videos with up to 100% needle

deployment detection rate and 97% frame classification accuracy. Prior knowledge of needle deployment geometry and EM-tracked US probe motion helped to reduce the number of false positives dramatically. The algorithm can be used to reliably eliminate the vast majority of frames without needle deployments and thus greatly accelerate the review of the video sequences.

In our future work, we will try to further reduce the false positive rate for the needle detection. By analyzing our current results, it was noticed that the false positives were largely due to either the needle traces left in the prostate after that the needle was withdrawn or the motion artifacts of the prostate. The former may be addressed by checking the tracked US probe position, since the same location should not be biopsied twice in a procedure. The latter may be handled by incorporating motion compensation to remove the global motion effects from the TRUS video.

## References

- [1] American Cancer Society, Prostate cancer. <http://www.cancer.org/>; 2008.
- [2] Chen V, Mouraviev V, Mayes J, Sun L, Madden J, Moul J, et al. Utility of a 3-dimensional transrectal ultrasound-guided prostate biopsy system for prostate cancer detection. *Technol Cancer Res Treat* 2009;8(2):99–104.
- [3] Kruecker J, Xu S, Glossop N, Guion P, Choyke P, Singh A, et al. Fusion of real-time transrectal ultrasound with pre-acquired MRI for multimodality prostate imaging. In: *Visualization, Image-guided Procedures, and Display*, vol. 6509 of *SPIE Medical Imaging*. 2007. p. 650912.
- [4] Xu S, Kruecker J, Guion P, Glossop N, Neeman Z, Choyke P, et al. Closed-loop control in fused MR-TRUS image-guided prostate biopsy. In: *MICCAI*, vol. 4791 of *LNCS*. 2007. p. 128–35.
- [5] Wei Z, Gardi L, Downey D, Fenster A. Oblique needle segmentation for 3D TRUS-guided robot-aided transperineal prostate brachytherapy. In: *IEEE International Symposium on Biomedical Imaging: Nano to Macro*, 2004. 2004. p. 960–3.
- [6] Wei Z, Gardi L, Downey D, Fenster A. Oblique needle segmentation and tracking for 3D TRUS guided prostate brachytherapy. *Med Phys* 2005;32:2928.
- [7] Draper K, Blake C, Gowman L, Downey D, Fenster A. An algorithm for automatic needle localization in ultrasound-guided breast biopsies. *Med Phys* 2000;27:1971.
- [8] Ding M, Fenster A. A real-time biopsy needle segmentation technique using hough transform. *Med Phys* 2003;30:2222–33.
- [9] Okazawa S, Ebrahimi R, Chuang J, Rohling R, Salcudean S. Methods for segmenting curved needles in ultrasound images. *Med Image Anal* 2006;10(3):330–42.
- [10] Hartmann P, Baumhauer M, Rassweiler J, Meinzer H. Automatic needle segmentation in 3D ultrasound data using a hough transform approach, *Bildverarbeitung Für Die Medizin 2009: Algorithmen-Systeme-Anwendungen*; 2009. p. 341.
- [11] Boykov Y, Veksler O, Zabih R. Fast approximate energy minimization via graph cuts. *IEEE Trans Pattern Anal Mach Intell* 2001;23(11):1222–39.
- [12] Kolmogorov V, Zabih R. What energy functions can be minimized via graph cuts? *IEEE Trans Pattern Anal Mach Intell* 2004;26(2):147–59.
- [13] Boykov Y, Kolmogorov V. An experimental comparison of min-cut/max-flow algorithms for energy minimization in vision. *IEEE Trans Pattern Anal Mach Intell* 2004;26(9):1124–37.